TITLE: A protective broadly cross-reactive human antibody defines a conserved site of vulnerability on beta-coronavirus spikes

SUMMARY: A human mAb isolated from a COVID-19 donor defines a protective cross-neutralizing epitope promising for pan-β-CoV vaccine strategies

AUTHORS:
Panpan Zhou[1,3,4,*], Meng Yuan[2,*], Ge Song[1,3,4,*], Nathan Beutler[1,*], Namir Shaabani[1,*], Deli Huang[1], Wan-ting He[1,3,4], Xueyong Zhu[2], Sean Callaghan[1,3,4], Peter Yong[1,3,4], Fabio Anzanello[1,3,4], Linghang Peng[1], James Ricketts[1], Mara Parren[1], Elijah Garcia[1], Stephen A. Rawlings[5], Davey M. Smith[5], David Nemazee[1], John R. Teijaro[1], Thomas F. Rogers[1,5,†], Ian A. Wilson[2,3,4,6,†], Dennis R. Burton[1,3,4,7,†], Raiees Andrabi[1,3,4,†]

AUTHORS AFFILIATIONS:
[1]Department of Immunology and Microbiology, The Scripps Research Institute, La Jolla, CA 92037, USA.
[2]Department of Integrative Structural and Computational Biology, The Scripps Research Institute, La Jolla, CA 92037, USA.
[3]IAVI Neutralizing Antibody Center, The Scripps Research Institute, La Jolla, CA 92037, USA
[4]Consortium for HIV/AIDS Vaccine Development (CHAVD), The Scripps Research Institute, La Jolla, CA 92037, USA.
[5]Division of Infectious Diseases, Department of Medicine, University of California, San Diego, La Jolla, CA 92037, USA.
[6]Skaggs Institute for Chemical Biology, The Scripps Research Institute, La Jolla, CA 9203
[7]Ragon Institute of Massachusetts General Hospital, Massachusetts Institute of Technology, and Harvard University, Cambridge, MA 02139, USA.
[*]These authors contributed equally to this work.
[†]Corresponding author. Email: trogers@sscripp.edu (T.F.R.); wilson@scripps.edu (I.A.W); burton@scripps.edu (D.R.B.); andrabi@scripps.edu (R.A.).

ABSTRACT

We recently described CC40.8 bnAb from a COVID-19 donor that exhibits broad reactivity with human β-CoVs. Here, we show that CC40.8 targets the conserved S2 stem-helix region of the coronavirus spike fusion machinery. We determined a crystal structure of CC40.8 Fab with a SARS-CoV-2 S2 stem-peptide at 1.6 Å resolution and found that the peptide adopts a mainly helical structure. Conserved residues in β-CoVs interact with the antibody, thereby providing a molecular basis for its broad reactivity. CC40.8 exhibits *in vivo* protective efficacy against SARS-CoV-2 challenge in a hamster model with reduction in weight loss and lung viral titers. Furthermore, we noted CC40.8-like bnAbs are relatively rare in human COVID-19 infection and therefore their elicitation may require rational vaccine strategies. Overall, our study describes a new target on CoV spikes for protective antibodies that may facilitate the development of pan-β-CoV vaccines.

MAIN TEXT

Introduction

Severe acute respiratory syndrome coronavirus 2 (SARS-CoV-2) has led to the current global pandemic (*1-3*). SARS-CoV-2 is a novel virus that belongs to the coronaviridae family of which previously six members have crossed into humans and established widespread infections (*4, 5*). These include four endemic human coronaviruses (HCoVs) (HCoV-229E, HCoV-HKU1, HCoV-OC43, HCoV-NL63) responsible for non-severe, seasonal infections (*4*) and SARS-CoV-1 and MERS-CoV (Middle East Respiratory Syndrome CoV) that are associated with high morbidity and mortality in humans (*6, 7*). Among the seven HCoVs, SARS-CoV-2 closely resembles SARS-CoV-1 and to lesser degree MERS-CoV. Together with HCoV-HKU1 and HCoV-OC43, these viruses belong to the *betacoronavirus* genus (*4, 5*). SARS-CoV-2 is highly transmissible in humans and causes coronavirus disease 2019 (COVID-19), associated with severe respiratory failure leading to high morbidity and a reported mortality of ~0.7-2% infected individuals worldwide (*2, 8, 9*). These coronaviruses have crossed into humans through zoonotic transmissions from animal reservoirs highlighting the threat for future spillovers (*10-15*).

Coronavirus pandemic preparedness largely contemplates responding to viruses as they emerge as rapidly as possible and containment or mitigation to control spread. An alternative is to seek to identify broadly neutralizing antibodies (bnAbs) to coronaviruses and use molecular information on their epitopes to rationally design pan-coronavirus vaccines (*16-18*). Such vaccines could be stockpiled ahead of the emergence of a new

coronavirus and used to rapidly contain the virus. BnAbs and pan-coronavirus vaccines that target more conserved regions of the viruses may also be more effective against variant viruses, for example that are now being observed in the COVID-19 pandemic (*19-21*).

All HCoVs possess a surface envelope spike glycoprotein that mediates interaction with host cell receptors and enables virus fusion (*4, 22*). SARS-CoV-2 (similar to SARS-CoV-1) utilizes the receptor binding domain (RBD) in the S1 subunit of the spike to engage human angiotensin converting enzyme 2 (hACE2) on host cells for cell entry and infection (*22-26*). The SARS-CoV-2 spike glycoprotein is the primary target of nAbs (*27-30*). On the spike protein, the RBD is highly immunogenic and is recognized by the majority of nAbs (*27, 31-42*), and thus is a major focus of current nAb-based vaccine design efforts (*27, 43, 44*). However, due to sequence diversity, cross-reactivity to the RBD region is limited, especially among the emerging coronaviruses with pandemic potential (*10-13*). As the rapid spread of the SARS-CoV-2 virus continues and the fact that most humans make potent nAbs to epitopes overlapping the ACE2 binding site, these epitopes appear to be under strong immune selection pressure at the population level that is leading to the selection of SARS-CoV-2 neutralization escape variants (*19-21, 45-47*). Such mutations may result in reduced effectiveness of vaccine-induced antibody responses in humans. The most striking example that illustrates the capability of the RBD to mutate without majorly affecting the ability of the virus to engage host receptor is the variability of the RBD across the two families of HCoVs: SARS-CoV-2/1 (β-HCoVs) and HCoV-NL63 (α-HCoV) (*22-26, 48*). These HCoVs possess divergent RBDs, but all use the ACE2 receptor

for viral entry suggesting that SARS-CoV-2 and potentially other emerging sarbecoviruses with human pandemic potential can tolerate changes in this domain with limited fitness cost. Therefore, we believe that other sites on the S protein should be explored as targets of (b)nAbs.

From a COVID-19 donor, we recently isolated a SARS-CoV-1/2 cross-neutralizing antibody, CC40.8, that exhibits broad cross-reactivity with human β-CoVs (*49*). Here, we show that the CC40.8 bnAb targets an S2 stem-helix epitope, which is part of the coronavirus fusion machinery. We first identified an extended 25-mer S2 peptide from HCoV-HKU1 that bound CC40.8 with high affinity and then determined the crystal structure of CC40.8 with the SARS-CoV-2 S2 peptide. The S2 stem peptide adopts a helical structure that is embedded in a groove between heavy and light chain CDRs. The epitope contact residues were confirmed, by alanine scanning, to be important for peptide binding and for virus neutralization. These contact residues are largely conserved between β-CoVs, consistent with the cross reactivity of CC40.8. In a SARS-CoV-2 hamster challenge model, CC40.8 showed *in vivo* protective efficacy by reducing weight loss and lung tissue viral titers. Although two recent studies have described S2-stem nAbs isolated from mice and mice transgenic for human Ig (*50, 51*), CC40.8 represents the first human HCoV S2-stem directed bnAb isolated from natural infection and may facilitate development of antibody-based interventions and prophylactic pan-sarbecovirus vaccine strategies.

Results

Broadly neutralizing antibody (bnAb) CC40.8 binds a conserved peptide from the S2 region of beta-coronaviruses

We recently isolated a bnAb, CC40.8, from a SARS-CoV-2-infected donor that neutralizes SARS-CoV-1 and SARS-CoV-2 and exhibits broad reactivity against β-coronaviruses, notably the endemic coronavirus HCoV-HKU1 (Fig. 1A-B)(*49*). We investigated and observed that CC40.8 bnAb prevents cell-cell fusion of HeLa cells expressing either SARS-CoV-2 spike or hACE2 receptor (Fig. S1). Using negative-stain electron microscopy (ns-EM), we previously showed that the CC40.8 antibody targets the base of the S2 subunit on HCoV S proteins but epitope flexibility precluded determination of a high-resolution structure (*49*). Here, we pursued epitope identification first by peptide mapping. Using HCoV-HKU1 S2 subunit overlapping biotinylated peptides (15-residue long with a 10-residue overlap) for binding to CC40.8, we identified that stem-helix region in the S2 fusion domain contains the epitope (Fig. 1C, Fig. S2). Then, through screening with peptides of various lengths that include the epitope, we identified a 25-residue peptide that showed the strongest binding by BLI (Fig. 1D upper panel). The peptide corresponds to residues 1226-1250 from the HCoV-HKU1 S2 sequence.

Next, we tested BLI binding of CC40.8 bnAb with peptides encompassing similar S2-domain regions of other HCoVs and observed that the antibody binds to the β- but not to the α-HCoV S2-domain peptides (Fig. 1D, lower panel). This pattern is consistent with

the differential binding of CC40.8 bnAb to different families of HCoV S proteins (Fig. 1B) (*49*). Sequence alignment of the S2 stem-helix domain region showed strong conservation between SARS-CoV-1 and SARS-CoV-2 with more modest conservation across the seasonal β-CoVs, consistent with cross-reactive binding patterns (Fig. 1E-F) (compare also Fig 3C below).

The epitope of CC40.8 bnAb defined by the crystal structure of a peptide-antibody complex

To investigate the molecular nature of the CC40.8 bnAb epitope, we determined the 1.6 Å resolution crystal structure of the antibody Fab fragment with the SARS-CoV-2 25-mer S2 peptide (Fig. 2A, Table S2). The peptide adopts a largely helical structure that traverses a wide hydrophobic groove formed between the heavy and light chains of the Fab (Fig. 2A-C). The buried surface area on the peptide is ~1150 $Å^2$ (669 $Å^2$ conferred by the heavy chain and 488 $Å^2$ by the light chain) and is largely contributed by hydrophobic residue interactions at the paratope/epitope interface, although some hydrogen bonds and salt bridges are contributed by CDRH1-3, FRH1, and CDRL1-3 (Fig. 2A-C, Fig 3A-B). Two peptide stretches of ^{1142}QPELD^{1146} and ^{1151}ELDKYF^{1156} and several nearby residues, F^{1148} N^{1158}, H^{1159}, form the epitope of the bnAb (Fig. 3A-B). Notably, hydrophobic residues in ^{1151}ELDKYF^{1156} of the stem region as well as two upstream residues, L^{1145} and F^{1148}, form the core of the epitope that interacts with a hydrophobic groove in the antibody lined by heavy chain residues (V33, Y35, W47, Y56, Y58, M96 and V101) and light chain residues (Y32, Y34, L46 and Y49) (Fig. 3B and Fig. S3).

Antibody germline and mutated residues both contribute to epitope recognition (Fig. S3). Consistent with our findings, two recent independent studies have shown that heterologous CoV S protein immunizations in mice or mice transgenic for the human Ig locus can induce cross-reactive serum neutralizing antibodies that target the conserved S2 spike epitope similar to the stem-helix epitope identified in our study, and some isolated mAbs also show broad reactivity to coronavirus spikes (*50, 51*).

The residues important for CC40.8 interaction with virus were also investigated by alanine scanning mutagenesis of SARS-CoV-2 and HCoV-HKU1 peptides and spike protein by antibody binding and by neutralization of SARS-CoV-2 spike mutants (Fig. 3D-E, Fig. S4). The contact residues determined by crystallography were also found to be important for peptide binding and neutralization with the S2 helical residues, L^{1145}, E^{1151}, and Y^{1155}, being the most critical (Fig. S4). The CC40.8 bnAb epitope appears to be only partially exposed on HCoV S protein (Fig. S5).

The conservation of those residues identified by crystallography and alanine scanning as most critical for interaction of CC40.8 with virus is high (Fig 3C) across human β-coronaviruses and related sarbecoviruses that infect various animal species, thus providing a structural basis for broad cross-reactivity of the antibody (Fig. 3C).

The CC40.8 epitope region houses an N-linked glycan (N^{1158}) that is highly conserved across coronaviruses and may restrict access to this bnAb epitope. To investigate, we substituted the T^{1160} residue on SARS-CoV-2 virus spike with an alanine residue to

eliminate the NHT glycan site. A modest increase in neutralization sensitivity of the T1160A variant relative to wild-type virus was observed (Fig. 3E, Fig. S4), suggesting that any steric obstruction of the epitope by the N1158 glycan is limited.

CC40.8 antibody protects against weight loss and reduces viral burden in *in vivo* SARS-CoV-2 challenge

To determine the *in vivo* efficacy of CC40.8, we conducted a passive antibody transfer followed by SARS-CoV-2 challenge in Syrian hamsters. CC40.8 mAb was intra-peritoneally (i.p.) administered into a group of 5 Syrian hamsters at 2 mg per animal (Fig. 4A). An unrelated antibody to Zika virus, Zikv mAb1, was i.p. administered into 5 Syrian hamsters used as a control group. Animals in both groups were challenged with SARS-CoV-2 (USA-WA1/2020) by intranasal (i.n.) administration of a virus dose of 1×10^6 plaque forming units (PFU), 12 hours post antibody infusion (Fig. 4A). The animals were weighed daily to monitor weight changes, as an indicator of disease due to the infection. Animals were sacrificed at day 5 and the lung tissues were collected to determine the SARS-CoV-2 titers by plaque assay. The CC40.8 bnAb-treated animals showed substantially reduced weight loss as compared to the Zikv mAb1 treated control group animals (Fig. 4B), suggesting a protective role of CC40.8. Consistent with this result, the SARS-CoV-2 titers in lung tissues were significantly reduced ($p = 0.01$) in the CC40.8-treated animals compared to the control group animals (Fig. 4C). Notably, 3 out of 5 animals in the CC40.8-treated group showed complete viral clearance in lung tissues at day 5. Altogether, the findings reveal that CC40.8, despite relatively low *in vitro*

neutralization potency, shows a substantial level of protective efficacy against SARS-CoV-2 infection *in vivo*. This phenomenon of a surprisingly high level of protection afforded by antibodies directed to epitopes close to the spike membrane and part of the fusion machinery has been described earlier for HIV (*52*).

The conserved stem-helix epitope defined by bnAb CC40.8 is infrequently targeted following SARS-CoV-2 infection

To investigate how frequently the CC40.8 epitope is targeted following SARS-CoV-2 infection, we tested the binding of sera from 60 COVID-19 convalescent donors to 25-mer peptides of HCoVs corresponding to the stem-helix bnAb epitope. We observed that 6/60 (10%) individuals exhibited some level of cross-reactive binding with β-HCoV S2 stem peptides (Fig. 5A). We further tested the binding of cross-reactive sera with SARS-CoV-2 S2 stem peptide alanine scan variants spanning the CC40.8 epitope and observed the presence of CC40.8-like epitope-targeting antibodies (Fig. 5B). The binding of cross-reactive serum Abs revealed dependence on five common stem helix residues including a conserved hydrophobic core formed by residues, F^{1148}, L^{1152}, Y^{1155} and F^{1156} (Fig. 5B). To determine the contribution of S2-stem directed nAbs in overall SARS-CoV-2 neutralization by serum Abs in cross-reactive COVID-19 donors, we conducted competition experiments with the SARS-CoV-2 S2 stem-helix peptide. Peptide competition showed no or minimal effects on the SARS-CoV-2 neutralization (Fig. 5C), suggesting that stem-helix targeting cross-reactive nAbs minimally contribute to the overall polyclonal serum neutralization in these COVID-19 convalescent donors.

Discussion

The development of effective pan-coronavirus vaccine strategies that can mitigate future outbreaks from new emerging coronaviruses is important (*16, 18*). Two major challenges are: i) the identification of broadly neutralizing antibody (bnAb) targets on CoV spikes; and ii) the development of novel vaccine strategies that can reproducibly induce durable and protective pan-CoV bnAbs. The approach of identifying conserved bnAb surface protein targets by isolating bnAbs from natural infection and utilizing their molecular information in structure-guided immunogen design has greatly contributed to the development of vaccine strategies against a range of complex pathogen surfaces (*53-60*).

The spike S1 subunit shows considerable variation on HCoVs, while the S2 subunit is relatively more conserved, especially across the β-HCoVs and appears to be promising for developing pan-CoV bnAb vaccine strategies. Accordingly, we recently isolated a SARS-CoV-1/2 cross-neutralizing Ab, CC40.8, that exhibits broad reactivity with human β-CoVs (*49*). In this study, using epitope mapping and structural studies, we determined the spike epitope recognized by CC40.8, which represents the first S2 domain SARS-CoV-2 cross-neutralizing epitope defined with a human antibody elicited in natural infection. The epitope forms a stem-helix structure conserved across coronaviruses and may thus serve as a promising target for pan-coronavirus vaccine strategies. The epitope is highly enriched in hydrophobic residues as well as some charged residues and the

bnAbs targeting this region may neutralize by sterically interfering with the fusion machinery (*50, 51*), suggesting a potential target for fusion inhibitors (*61-63*).

We noted that cross-reactive antibodies directed to CC40.8 S2 stem-helix epitope are relatively less frequently elicited in human coronavirus natural infections as compared to strain-specific neutralizing antibody responses (*27*). However, a few recent studies using more sensitive antibody detection assays have revealed higher prevalence of polyclonal stem-helix region-directed antibodies in COVID-19 donors and their association with reduced disease severity (*64-66*). Regardless, the small subset of individuals in our sample cohort that do make cross-reactive Abs, seem to exhibit broad reactivity to human β-coronaviruses, which is promising for pan-coronavirus vaccine strategies. It however remains to be determined whether the paucity of these cross-reactive antibodies is due to poor accessibility of the S2 stem-helix epitope on the native spike, low frequency of bnAb-encoding B cell precursors in humans, or complex secondary B cell maturation pathways. Thus, isolation of multiple cross-reactive pan-CoV bnAb lineages, understanding their maturation pathways, and identifying common antibody framework motifs that could be targeted by rational vaccine design approaches may be important (*67*). Encouragingly, two recent studies have described a similar CoV S2 domain bnAb epitope being targeted by cross-reactive mAbs isolated from heterologous CoV S protein immunizations in mice and mice transgenic for the human Ig locus (*50, 51*). These data suggest that such bnAbs could be induced by both immunization with designed vaccines as well as coronavirus infection in humans. Nonetheless, it would need to be ascertained how many sequential immunizations would be needed to broaden the breadth of these

nAb responses. Encouragingly, despite relatively lower neutralization potency, the CC40.8 stem-helix directed nAb showed in vivo protective efficacy against SARS-CoV-2 challenge.

Overall, we describe a cross-neutralizing bnAb epitope on β-CoVs using a human bnAb and provided its molecular details that help explain the broad reactivity. The identification of the new coronavirus spike conserved epitope should facilitate bnAb-epitope based vaccine strategies and antibody-based intervention strategies against human coronaviruses and emerging coronaviruses with pandemic potential.

Acknowledgements

We thank all the human cohort participants for donating samples. This work was supported by the NIH CHAVD (UM1 AI44462 to D.R.B.) award, the IAVI Neutralizing Antibody Center, the Bill and Melinda Gates Foundation (OPP 1170236 and INV-004923 to I.A.W. and D.R.B.). This work was supported by the Translational Virology Core of the San Diego Center for AIDS Research (CFAR) grant number AI036214, a National Institutes of Health–funded program. S.A.R. was supported by the National Institutes of Health (grant number 5T32AI007384). This work was also supported by the John and Mary Tu Foundation and the Pendleton Trust.

Author contributions

P.Z., M.Y., G.S., I.A.W., D.R.B., and R.A. conceived and designed the study. N.B., J.R., M.P., E.G., S.A.R., D.M.S., and T.F.R. recruited donors and collected and processed plasma samples. P.Z., G.S., and F.A., performed BLI, ELISA and cell binding and virus neutralization assays. D.H., and L.P., conducted cell-cell fusion experiment. W.H., S.C., and P.Y., generated recombinant protein antigens. M.Y. and X.Z. determined crystal structure of the antibody-antigen complex. N.B., N.S., J.R.T., and T.F.R. carried out animal studies and viral load measurements. P.Z., M.Y., G.S., N.B., N.S., D.H., W.H., D.N., J.R.T., T.F.R., I.A.W., D.R.B., and R.A. designed the experiments and analyzed the data. R.A., P.Z., G.S., M.Y., I.A.W. and D.R.B. wrote the paper, and all authors reviewed and edited the paper.

Competing interests

Competing interests: R.A., G.S., W.H., T.F.R., and D.R.B. are listed as inventors on pending patent applications describing the SARS-CoV-2 and HCoV-HKU1 S cross-reactive antibodies. P.Z., G.S., M.Y., I.A.W., D.R.B. and R.A. are listed as inventors on a pending patent application describing the S2 stem epitope immunogens identified in this study. D.R.B. is a consultant for IAVI. All other authors have no competing interests to declare.

Figure and legends

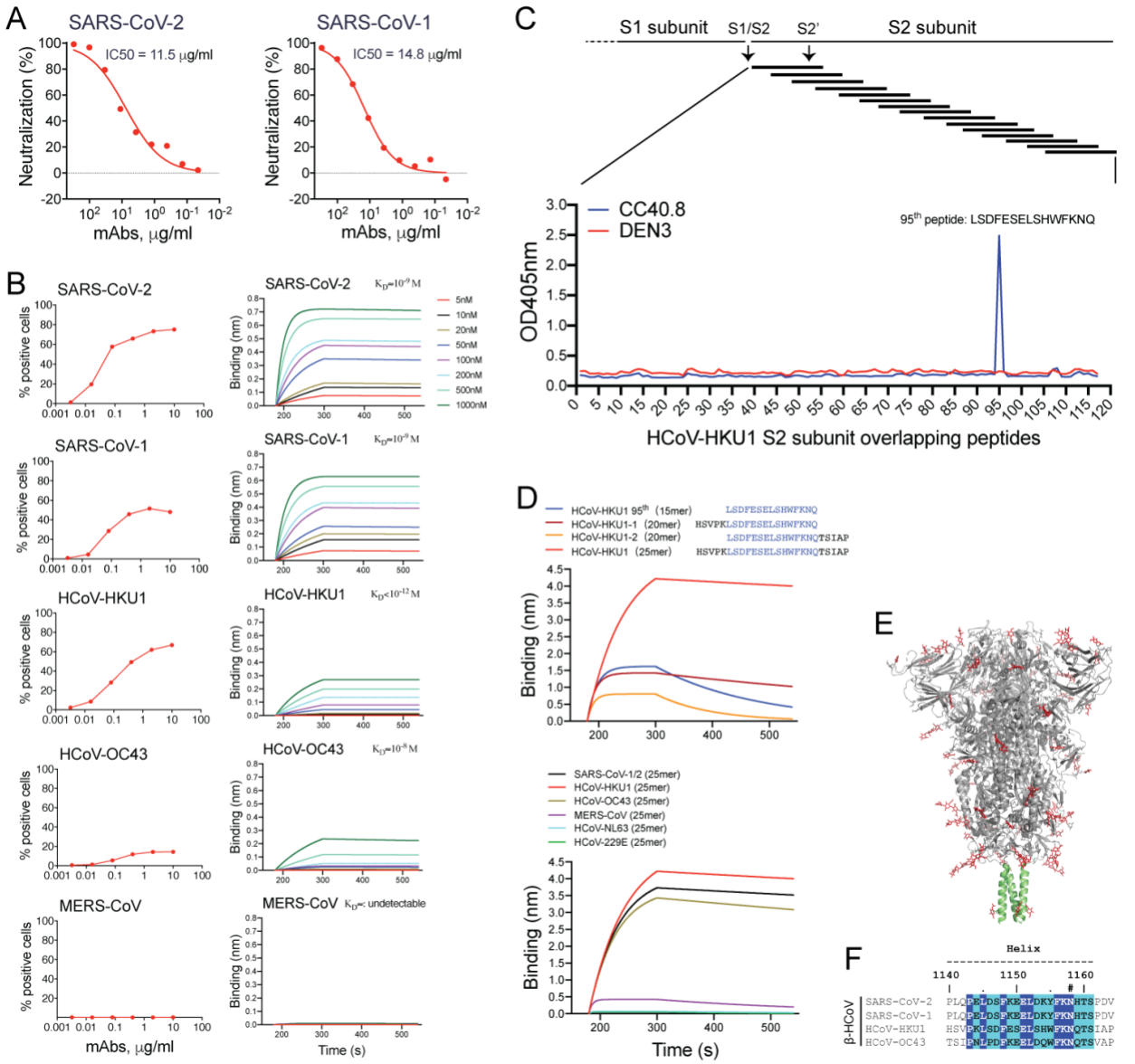

Figure 1. Identification of the CC40.8 bnAb epitope on the coronavirus spike by epitope mapping.

A. Neutralization of SARS-CoV-2 and SARS-CoV-1 by CC40.8 mAb isolated from a COVID-19 donor.

B. CELISA binding of CC40.8 mAb with β-HCoV spikes expressed on 293T cells. Binding to HCoV spikes is recorded as % positive cells using a flow cytometry method. CC40.8 mAb shows cross-reactive binding with 4 out of 5 human β-HCoV spikes. BioLayer Interferometry (BLI) binding of CC40.8 mAb with human β-HCoV soluble S proteins. Binding constants (KDs) for each Ab-antigen interaction are indicated.

C. Epitope mapping of CC40.8 with HCoV-HKU1 S2 subunit overlapping peptides. A series of HCoV-HKU1 S2 overlapping biotinylated peptides (15-residue long with a 10-residue overlap) were tested for binding to CC40.8 mAb by ELISA. CC40.8 showed

binding to the 95th 15-mer peptide corresponding to the HCoV-HKU1 S2 stem-helix region (residue position range: 1231-1245). An unrelated antibody to dengue virus, DEN3, was a control.

D. BLI binding of CC40.8 to the HCoV-HKU1 95th 15-mer stem peptide (blue) and HCoV-HKU1 stem peptide variants with 5 additional residues either at the N-(20-mer: brick red) or C-(20-mer: orange) terminus or added at both termini (25-mer: red). CC40.8 showed strongest binding to the 25-residue stem peptide corresponding to HCoV-HKU1 S2 residues 1126-1150. BLI binding of CC40.8 to 25-mer stem peptides derived from all HCoV spikes. CC40.8 showed binding to the β- but not to the α-HCoV S2 stem peptides.

E. SARS-CoV-2 S protein cartoon depicting the S2-stem epitope region in green at the base of the prefusion spike.

F. Sequence conservation of CC40.8 stem-helix epitope on SARS-CoV-1/2, HCoV-HKU1 and HCoV-OC43 human β-CoV spikes. Conserved residues are highlighted with blue boxes, while similar residues in cyan boxes. An N-linked glycosylation site is indicated with a “#” symbol.

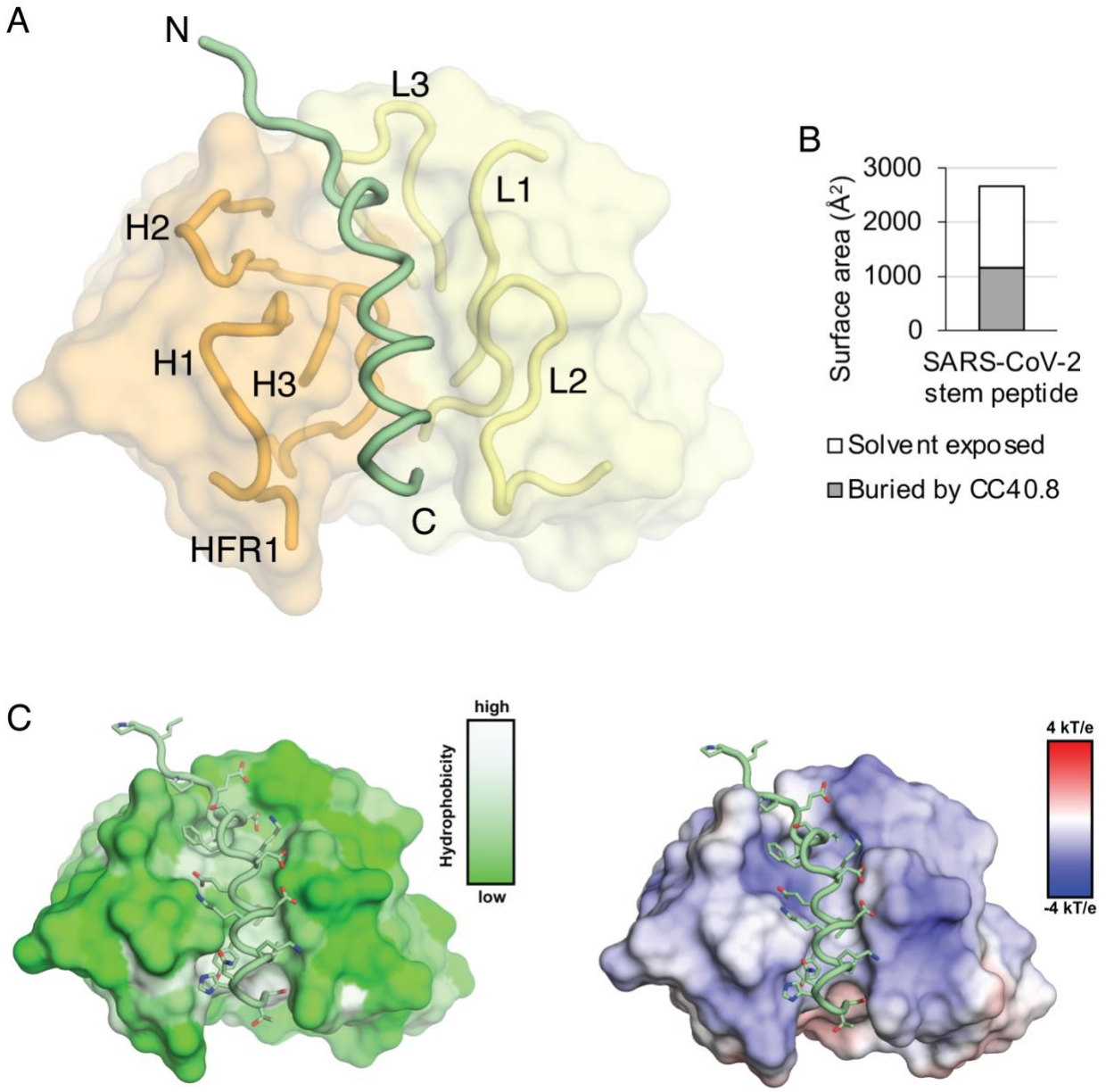

Figure 2. Crystal structure of CC40.8 antibody in complex with the SARS-CoV-2 stem peptide.

A. Overall view of the CC40.8-peptide complex structure. Heavy and light chains of CC40.8 are shown in orange and yellow semi-transparent surfaces, respectively, where paratope regions are shown as cartoon. The SARS-CoV-2 stem-helix peptide is shown in green.

B. Surface area of the SARS-CoV-2 stem peptide. Solvent exposed and buried areas were calculated with Proteins, Interfaces, Structures and Assemblies (PISA) (*68*).

C. The SARS-CoV-2 stem peptide inserts into a hydrophobic groove formed by the heavy and light chains of CC40.8. Surfaces of CC40.8 are color-coded by hydrophobicity [calculated by Color h (https://pymolwiki.org/index.php/Color_h)].

D. Electrostatic surface potential of the CC40.8 paratope. Electrostatic potential is calculated by APBS and PDB2PQR (*69, 70*).

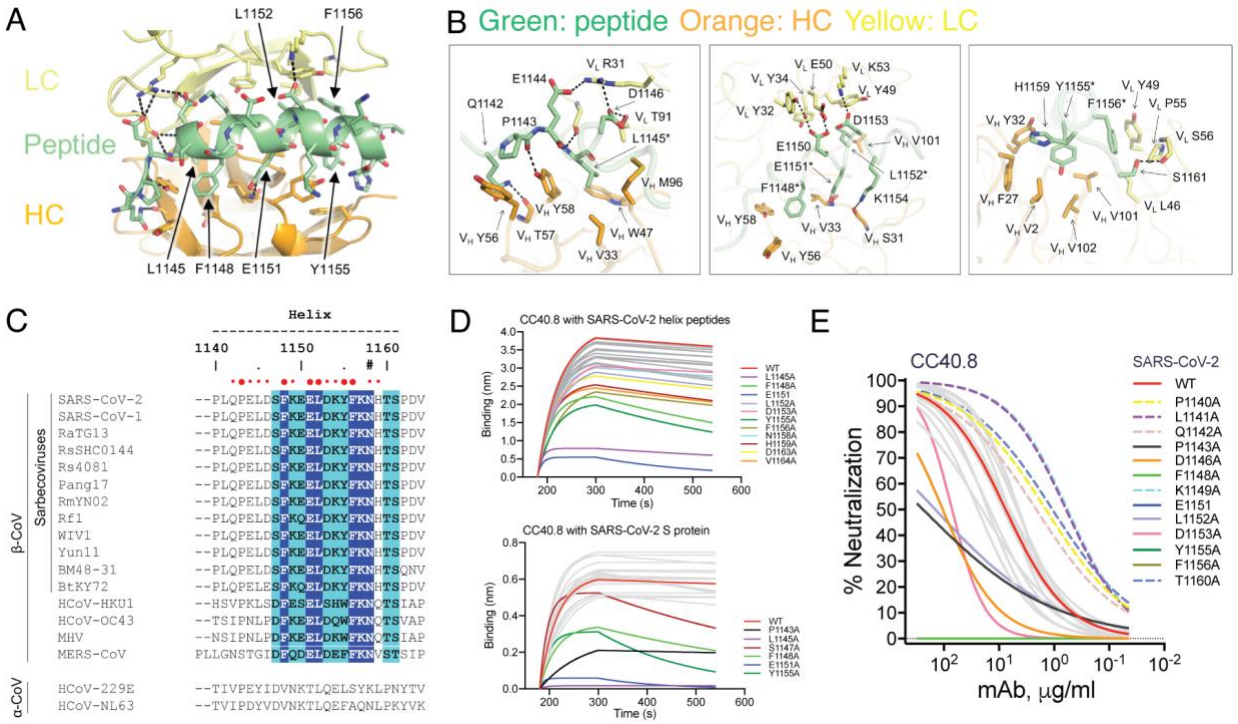

Figure 3. Crystal structure showing the S2 stem residues involved in contact with CC40.8 and their conservation across CoVs.

A. An overall view of the CC40.8 antibody and S2 stem-peptide interaction. Heavy and light chains of CC40.8 are shown in orange and yellow, respectively, whereas the SARS-CoV-2 stem peptide is in green. Hydrogen bonds and salt bridges are represented by black dashed lines.

B. Details of interactions between CC40.8 and the SARS-CoV-2 stem peptide. Residues conserved in SARS-CoV-1, SARS-CoV-2, HCoV-HKU-1, and HCoV-OC43 are labeled with asterisks (*).

C. Sequence conservation of CC40.8 stem-helix epitope on SARS-CoV-1/2, sarbecoviruses infecting other animal species, human β-CoVs and mouse hepatitis virus (MHV). The stem region forming the helix and the residues involved in interaction with CC40.8 antibody are indicated by red dots (cutoff distance = 4 Å) , within which bigger dots indicate residues that are essential for CC40.8 interaction, where alanine scanning mutagenesis of such residue decreased neutralization IC50 for at least 10 folds or a complete knock-out (details are shown in Fig. S4). Conserved residues are highlighted with blue boxes, while similar residues in cyan boxes. An N-linked glycosylation site is indicated with a "#" symbol. The region presents a helical secondary structure in the CC40.8/peptide structure is indicated on top of the panel.

D. BLI binding of CC40.8 bnAb to SARS-CoV-2 stem-helix peptide and soluble spike alanine mutants spanning the whole epitope. The stem peptide or spike mutants that substantially affect CC40.8 bnAb binding are shown in colors.

E. CC40.8 neutralization of SARS-CoV-2 and the stem-helix alanine mutants spanning the whole epitope. The virus mutants that substantially affect CC40.8 bnAb neutralization are shown in colors.

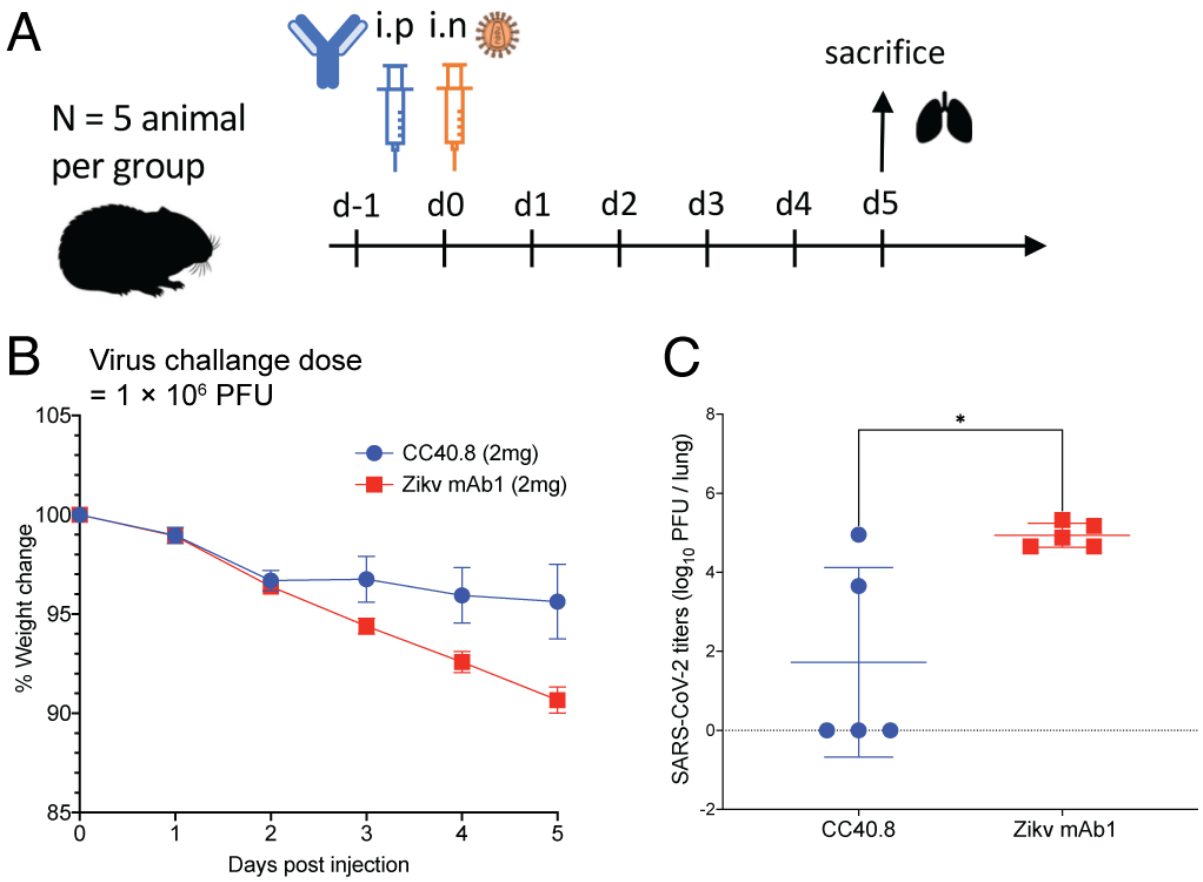

Figure 4. CC40.8 reduces weight loss and lung viral replication following SARS-CoV-2 challenge in Syrian hamsters.

A. CC40.8 was intraperitonially (i.p.) administered at 2 mg per animal dose into Syrian hamsters (average: 16.5 mg/kg). Control animals received 2 mg of control Zikv mAb1. Each group of five animals was challenged intranasally (i.n.) 12 hours after antibody infusion with 1 × 10^6 PFU of SARS-CoV-2. Animal weight was monitored daily as an indicator of disease progression and lung tissue was collected on day 5 for viral burden assessment.

B. Percent weight change in CC40.8 or control antibody-treated animals after SARS-CoV-2 challenge. Percent weight change was calculated from day 0 for all animals.

C. SARS-CoV-2 titers (PFU) as determined by plaque assay from lung tissue at day 5 after infection.

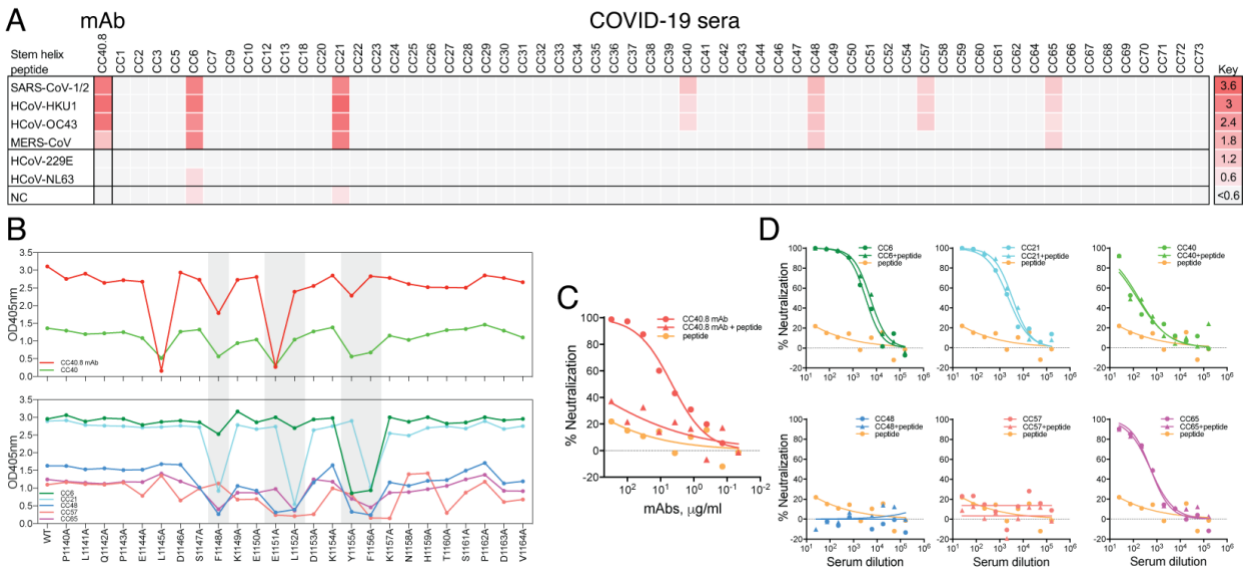

Figure 5. Frequency of CC40.8 S2 epitope-targeting serum antibodies in human COVID-19 donors.

A. Heatmap showing ELISA binding reactivity profiles of convalescent COVID sera with 25-mer peptides corresponding to the CC40.8 bnAb S2 epitopes on human β-(SARS-CoV-2, SARS-CoV-1, MERS-CoV, HCoV-HKU1, HCoV-OC43) and α-(HCoV-NL63 and HCoV-229E) coronaviruses. The extent of binding is color coded with red indicating strong reactivity. CC40.8 mAb was the positive control for the binding assay and PBS-BSA solution served as the negative control. Six out of 60 COVID donors showed cross-reactive binding to various HCoV S peptides.

B. ELISA-based alanine scan epitope mapping of convalescent COVID-19 sera from CC6, CC21, CC40, CC48, CC57 and CC57 donors with SARS-CoV-2 stem peptides (25mer). CC40 sera showed dependence on similar SARS-CoV-2 stem helix residues as the CC40.8 mAb. SARS-CoV-2 stem helix residue positions targeted (decrease in ELISA binding compared to WT stem peptide) by multiple cross-reactive COVID-19 sera are shown in grey. Five residues, F^{1148}, E^{1151}, L^{1152}, Y^{1155} and F^{1156} were commonly targeted by the cross-reactive COVID-19 serum Abs. These residues form the stem-helix bnAb core epitope.

C. SARS-CoV-2 neutralization by CC40.8 in presence of competing SARS-CoV-2 stem peptide. Neutralization of SARS-CoV-2 by CC40.8 mAb, CC40.8 mAb pre-incubated with SARS-CoV-2 stem peptide (60ug/ml) and stem peptide-only control. The SARS-CoV-2 stem peptide inhibits the neutralizing activity of CC40.8 mAb.

D. SARS-CoV-2 neutralization by cross-reactive COVID-19 sera in presence of competing SARS-CoV-2 stem peptide. Neutralization of SARS-CoV-2 by sera from COVID-19 donors, CC6, CC21, CC40, CC48, CC57, CC57, sera pre-incubated with SARS-CoV-2 stem peptide (60ug/ml) and stem peptide only controls. The SARS-CoV-2 stem peptide had minimal effects on neutralization by stem-targeting COVID serum antibodies.

References

1. C. Huang *et al.*, Clinical features of patients infected with 2019 novel coronavirus in Wuhan, China. *Lancet* **395**, 497-506 (2020).
2. Z. Wu, J. M. McGoogan, Characteristics of and Important Lessons From the Coronavirus Disease 2019 (COVID-19) Outbreak in China: Summary of a Report of 72314 Cases From the Chinese Center for Disease Control and Prevention. *JAMA*, (2020).
3. P. Zhou *et al.*, A pneumonia outbreak associated with a new coronavirus of probable bat origin. *Nature* **579**, 270-273 (2020).
4. J. Cui, F. Li, Z. L. Shi, Origin and evolution of pathogenic coronaviruses. *Nat Rev Microbiol* **17**, 181-192 (2019).
5. T. S. Fung, D. X. Liu, Human Coronavirus: Host-Pathogen Interaction. *Annu Rev Microbiol* **73**, 529-557 (2019).
6. C. Drosten *et al.*, Identification of a novel coronavirus in patients with severe acute respiratory syndrome. *The New England journal of medicine* **348**, 1967-1976 (2003).
7. A. M. Zaki, S. van Boheemen, T. M. Bestebroer, A. D. Osterhaus, R. A. Fouchier, Isolation of a novel coronavirus from a man with pneumonia in Saudi Arabia. *The New England journal of medicine* **367**, 1814-1820 (2012).
8. E. Petersen *et al.*, Comparing SARS-CoV-2 with SARS-CoV and influenza pandemics. *Lancet Infect Dis* **20**, e238-e244 (2020).
9. G. Meyerowitz-Katz, L. Merone, A systematic review and meta-analysis of published research data on COVID-19 infection fatality rates. *Int J Infect Dis* **101**, 138-148 (2020).
10. N. Wang *et al.*, Serological Evidence of Bat SARS-Related Coronavirus Infection in Humans, China. *Virol Sin* **33**, 104-107 (2018).
11. V. D. Menachery *et al.*, SARS-like WIV1-CoV poised for human emergence. *Proceedings of the National Academy of Sciences of the United States of America* **113**, 3048-3053 (2016).
12. V. D. Menachery *et al.*, A SARS-like cluster of circulating bat coronaviruses shows potential for human emergence. *Nature medicine* **21**, 1508-1513 (2015).
13. M. Letko, A. Marzi, V. Munster, Functional assessment of cell entry and receptor usage for SARS-CoV-2 and other lineage B betacoronaviruses. *Nat Microbiol* **5**, 562-569 (2020).
14. S. J. Anthony *et al.*, Further Evidence for Bats as the Evolutionary Source of Middle East Respiratory Syndrome Coronavirus. *mBio* **8**, (2017).
15. X. Y. Ge *et al.*, Isolation and characterization of a bat SARS-like coronavirus that uses the ACE2 receptor. *Nature* **503**, 535-538 (2013).
16. D. R. Burton, E. J. Topol, Variant-proof vaccines - invest now for the next pandemic. *Nature* **590**, 386-388 (2021).
17. D. R. Burton, L. M. Walker, Rational Vaccine Design in the Time of COVID-19. *Cell host & microbe* **27**, 695-698 (2020).
18. W. C. Koff, S. F. Berkley, A universal coronavirus vaccine. *Science* **371**, 759 (2021).
19. J. R. Mascola, B. S. Graham, A. S. Fauci, SARS-CoV-2 Viral Variants-Tackling a Moving Target. *JAMA*, (2021).
20. P. Wang *et al.*, Antibody Resistance of SARS-CoV-2 Variants B.1.351 and B.1.1.7. *Nature*, (2021).
21. C. K. Wibmer *et al.*, SARS-CoV-2 501Y.V2 escapes neutralization by South African COVID-19 donor plasma. *bioRxiv*, (2021).
22. F. Li, Structure, Function, and Evolution of Coronavirus Spike Proteins. *Annu Rev Virol* **3**, 237-261 (2016).

23. F. Li, W. Li, M. Farzan, S. C. Harrison, Structure of SARS coronavirus spike receptor-binding domain complexed with receptor. *Science* **309**, 1864-1868 (2005).
24. A. C. Walls *et al.*, Structure, Function, and Antigenicity of the SARS-CoV-2 Spike Glycoprotein. *Cell* **181**, 281-292 e286 (2020).
25. D. Wrapp *et al.*, Cryo-EM structure of the 2019-nCoV spike in the prefusion conformation. *Science* **367**, 1260-1263 (2020).
26. H. Hofmann *et al.*, Human coronavirus NL63 employs the severe acute respiratory syndrome coronavirus receptor for cellular entry. *Proceedings of the National Academy of Sciences of the United States of America* **102**, 7988-7993 (2005).
27. L. Dai, G. F. Gao, Viral targets for vaccines against COVID-19. *Nature reviews. Immunology*, (2020).
28. F. Amanat, F. Krammer, SARS-CoV-2 Vaccines: Status Report. *Immunity* **52**, 583-589 (2020).
29. F. Krammer, SARS-CoV-2 vaccines in development. *Nature* **586**, 516-527 (2020).
30. S. F. Ahmed, A. A. Quadeer, M. R. McKay, Preliminary Identification of Potential Vaccine Targets for the COVID-19 Coronavirus (SARS-CoV-2) Based on SARS-CoV Immunological Studies. *Viruses* **12**, (2020).
31. D. F. Robbiani *et al.*, Convergent antibody responses to SARS-CoV-2 in convalescent individuals. *Nature* **584**, 437-442 (2020).
32. T. F. Rogers *et al.*, Isolation of potent SARS-CoV-2 neutralizing antibodies and protection from disease in a small animal model. *Science* **369**, 956-963 (2020).
33. A. Z. Wec *et al.*, Broad neutralization of SARS-related viruses by human monoclonal antibodies. *Science* **369**, 731-736 (2020).
34. B. Ju *et al.*, Human neutralizing antibodies elicited by SARS-CoV-2 infection. *Nature* **584**, 115-119 (2020).
35. R. Shi *et al.*, A human neutralizing antibody targets the receptor-binding site of SARS-CoV-2. *Nature* **584**, 120-124 (2020).
36. S. Du *et al.*, Structurally Resolved SARS-CoV-2 Antibody Shows High Efficacy in Severely Infected Hamsters and Provides a Potent Cocktail Pairing Strategy. *Cell* **183**, 1013-1023 e1013 (2020).
37. S. J. Zost *et al.*, Potently neutralizing and protective human antibodies against SARS-CoV-2. *Nature* **584**, 443-449 (2020).
38. Y. Wu *et al.*, A noncompeting pair of human neutralizing antibodies block COVID-19 virus binding to its receptor ACE2. *Science* **368**, 1274-1278 (2020).
39. P. J. M. Brouwer *et al.*, Potent neutralizing antibodies from COVID-19 patients define multiple targets of vulnerability. *Science* **369**, 643-650 (2020).
40. J. Hansen *et al.*, Studies in humanized mice and convalescent humans yield a SARS-CoV-2 antibody cocktail. *Science* **369**, 1010-1014 (2020).
41. C. O. Barnes *et al.*, Structures of Human Antibodies Bound to SARS-CoV-2 Spike Reveal Common Epitopes and Recurrent Features of Antibodies. *Cell* **182**, 828-842 e816 (2020).
42. Y. Cao *et al.*, Potent Neutralizing Antibodies against SARS-CoV-2 Identified by High-Throughput Single-Cell Sequencing of Convalescent Patients' B Cells. *Cell* **182**, 73-84 e16 (2020).
43. L. Premkumar *et al.*, The receptor binding domain of the viral spike protein is an immunodominant and highly specific target of antibodies in SARS-CoV-2 patients. *Sci Immunol* **5**, (2020).
44. M. Yuan *et al.*, Structural basis of a shared antibody response to SARS-CoV-2. *Science* **369**, 1119-1123 (2020).
45. E. Andreano *et al.*, SARS-CoV-2 escape in vitro from a highly neutralizing COVID-19 convalescent plasma. *bioRxiv*, 2020.2012.2028.424451 (2020).

46. Y. Weisblum *et al.*, Escape from neutralizing antibodies by SARS-CoV-2 spike protein variants. *Elife* **9**, (2020).
47. M. Yuan *et al.*, Structural and functional ramifications of antigenic drift in recent SARS-CoV-2 variants. *bioRxiv*, (2021).
48. K. Wu, W. Li, G. Peng, F. Li, Crystal structure of NL63 respiratory coronavirus receptor-binding domain complexed with its human receptor. *Proceedings of the National Academy of Sciences of the United States of America* **106**, 19970-19974 (2009).
49. G. Song *et al.*, Cross-reactive serum and memory B cell responses to spike protein in SARS-CoV-2 and endemic coronavirus infection. *bioRxiv*, 2020.2009.2022.308965 (2020).
50. M. M. Sauer *et al.*, Structural basis for broad coronavirus neutralization. *bioRxiv*, 2020.2012.2029.424482 (2021).
51. C. Wang *et al.*, Isolation of cross-reactive monoclonal antibodies against divergent human coronaviruses that delineate a conserved and vulnerable site on the spike protein. *bioRxiv*, 2020.2010.2020.346916 (2020).
52. D. R. Burton, A new lease on life for an HIV-neutralizing antibody class and vaccine target. *Proceedings of the National Academy of Sciences of the United States of America* **118**, (2021).
53. D. R. Burton, Antibodies, viruses and vaccines. *Nature reviews. Immunology* **2**, 706-713 (2002).
54. D. R. Burton, What Are the Most Powerful Immunogen Design Vaccine Strategies? Reverse Vaccinology 2.0 Shows Great Promise. *Cold Spring Harb Perspect Biol*, (2017).
55. S. F. Andrews, A. B. McDermott, Shaping a universally broad antibody response to influenza amidst a variable immunoglobulin landscape. *Curr Opin Immunol* **53**, 96-101 (2018).
56. G. Barba-Spaeth *et al.*, Structural basis of potent Zika-dengue virus antibody cross-neutralization. *Nature* **536**, 48-53 (2016).
57. D. Corti, A. Lanzavecchia, Broadly neutralizing antiviral antibodies. *Annual review of immunology* **31**, 705-742 (2013).
58. C. Dreyfus *et al.*, Highly conserved protective epitopes on influenza B viruses. *Science* **337**, 1343-1348 (2012).
59. A. I. Flyak *et al.*, Broadly neutralizing antibodies from human survivors target a conserved site in the Ebola virus glycoprotein HR2-MPER region. *Nat Microbiol* **3**, 670-677 (2018).
60. B. S. Graham, M. S. A. Gilman, J. S. McLellan, Structure-Based Vaccine Antigen Design. *Annu Rev Med* **70**, 91-104 (2019).
61. F. Vigant, N. C. Santos, B. Lee, Broad-spectrum antivirals against viral fusion. *Nat Rev Microbiol* **13**, 426-437 (2015).
62. R. U. Kadam, I. A. Wilson, Structural basis of influenza virus fusion inhibition by the antiviral drug Arbidol. *Proceedings of the National Academy of Sciences of the United States of America* **114**, 206-214 (2017).
63. D. Eggink, B. Berkhout, R. W. Sanders, Inhibition of HIV-1 by fusion inhibitors. *Curr Pharm Des* **16**, 3716-3728 (2010).
64. Y. Li *et al.*, Linear epitope landscape of the SARS-CoV-2 Spike protein constructed from 1,051 COVID-19 patients. *Cell reports*, 108915 (2021).
65. Y. Li *et al.*, Linear epitopes of SARS-CoV-2 spike protein elicit neutralizing antibodies in COVID-19 patients. *Cell Mol Immunol* **17**, 1095-1097 (2020).
66. J. T. Ladner *et al.*, Epitope-resolved profiling of the SARS-CoV-2 antibody response identifies cross-reactivity with an endemic human CoV. *bioRxiv*, (2020).
67. R. Andrabi, J. N. Bhiman, D. R. Burton, Strategies for a multi-stage neutralizing antibody-based HIV vaccine. *Curr Opin Immunol* **53**, 143-151 (2018).

68. E. Krissinel, K. Henrick, Inference of macromolecular assemblies from crystalline state. *Journal of molecular biology* **372**, 774-797 (2007).
69. E. Jurrus *et al.*, Improvements to the APBS biomolecular solvation software suite. *Protein science : a publication of the Protein Society* **27**, 112-128 (2018).
70. T. J. Dolinsky, J. E. Nielsen, J. A. McCammon, N. A. Baker, PDB2PQR: an automated pipeline for the setup of Poisson-Boltzmann electrostatics calculations. *Nucleic acids research* **32**, W665-667 (2004).

SUPPLEMENTARY ONLINE MATERIAL

Supplementary Materials

Materials and Methods
Table S1 – S2
Fig S1 – S5
References (1 – 12)

Materials and Methods

Human cohort information

Plasma from convalescent COVID-19 donors were kindly provided through the "Collection of Biospecimens from Persons Under Investigation for 2019-Novel Coronavirus Infection to Understand Viral Shedding and Immune Response Study" UCSD IRB# 200236. Samples were collected based on COVID-19 diagnosis regardless of gender, race, ethnicity, disease severity, or other medical conditions. The gender for individuals was evenly distributed across the human cohort. All human donors were assessed for medical decision-making capacity using a standardized, approved assessment, and voluntarily gave informed consent prior to being enrolled in the study. The summary of the demographic information of the COVID-19 donors is listed in Supplementary Table 1.

Pseudovirus production and generation of mutant spikes

Under BSL2/3 conditions, MLV-gag/pol and MLV-CMV plasmids were co-transfected into HEK293T cells along with full-length or variously truncated SARS-CoV1 and SARS-COV2 spike or mutant spike plasmids using Lipofectamine 2000 to produce single-round of infection competent pseudo-viruses. The medium was changed 16 hours post transfection. The supernatant containing MLV-pseudotyped viral particles was collected 48h post transfection, aliquoted and frozen at -80 °C for neutralization assay. Amino acid point mutations in SARS-CoV-2 spike encoding plasmids were made by using site-directed mutagenesis kit (NEB cat.# E0554S) according to the manufacturer's instructions. All the mutations were verified by DNA sequence analysis (Eton Bioscience, San Diego, CA).

Neutralization assay

Pseudotyped viral neutralization assay was performed as previously described with minor modification (Modified from TZM-bl assay protocol (*1*)). In sterile 96-well half-area plates, 25µl of virus was immediately mixed with 25 µl of three-fold serially diluted mAb (starting concentration of 300ug/ml) or serially diluted plasma from COVID-19 donors and incubated for one hour at 37°C to allow for antibody neutralization of the pseudotyped virus. Synthesized peptides were optionally added in the mixture for testing inhibition of neutralization. 10,000 HeLa-hACE2 cells/ well (in 50ul of media containing 20µg/ml Dextran) were directly added to the antibody virus mixture. Plates were incubated at 37°C for 42 to 48 h. Following the infection, HeLa-hACE2 cells were lysed using 1x luciferase lysis buffer (25mM Gly-Gly pH 7.8, 15mM MgSO4, 4mM EGTA, 1% Triton X-100). Luciferase intensity was then read on a Luminometer with luciferase substrate according to the manufacturer's instructions (Promega, PR-E2620). Percentage of neutralization was calculated using the following equation: 100 X (1 – (MFI of sample – average MFI of background) / average of MFI of probe alone – average MFI of

background)). Fifty percent maximal inhibitory concentrations (IC50), the concentrations required to inhibit infection by 50% compared to the controls, were calculated using the dose-response-inhibition model with 5-parameter Hill slope equation in GraphPad Prism 7(GraphPad Software, USA.)

CELISA binding

Binding of monoclonal antibody to various HCoV spikes expressed on the surface of HEK293T cells was determined by flow cytometry, as described previously (*2*). Briefly, HEK293T cells were transfected with different plasmids encoding full-length HCoV spikes and were incubated for 36-48 h at 37°C. Post incubation cells were trypsinized to prepare a single cell suspension and were distributed into 96-well plates. Monoclonal antibodies were prepared as 5-fold serial titrations in FACS buffer (1x PBS, 2% FBS, 1 mM EDTA), starting at 10ug/ml, 6 dilutions. 50 µl/well of the diluted samples were added into the cells and incubated on ice for 1h. The plates were washed twice in FACS buffer and stained with 50 µl/well of 1:200 dilution of R-phycoerythrin (PE)-conjugated mouse anti-human IgG Fc antibody (SouthernBiotech #9040-09) and 1:1000 dilution of Zombie-NIR viability dye (BioLegend) on ice in dark for 45min. After another two washes, stained cells were analyzed using flow cytometry (BD Lyrics cytometers), and the binding data were generated by calculating the percent (%) PE-positive cells for antigen binding using FlowJo 10 software.

Expression and purification of HCoV S proteins and SARS-CoV-2 S protein mutants

To express the soluble S ectodomain proteins, the HCoV S protein encoding plasmids were transfected into FreeStyle293F cells (Thermo Fisher). For general production, 350 ug plasmids were transfected into 1L FreeStyle293F cells at the density of 1 million cells/mL. 350 ug plasmids in 16ml transfectagro™ (Corning) were filtered and mixed with 1.8 mL 40K PEI (1mg/mL) in 16ml transfectagro™. After gently mixing the two components, the combined solution rested at room temperature for 30 min and was poured into 1L FreeStyle293F cell culture. The cell cultures were centrifuged at 2500xg for 15 min on day 4 after transfection, and the supernatants were filtered through the 0.22 µm membrane. The His-tagged proteins were purified with the HisPur Ni-NTA Resin (Thermo Fisher). Each column was washed with at least 3 bed volumes of wash buffer (25 mM Imidazole, pH 7.4), followed by elution with 25 ml of the elution buffer (250 mM Imidazole, pH 7.4) at slow gravity speed (~4 sec/drop). The eluates were buffer exchanged into PBS by using Amicon tubes, and the proteins were concentrated afterwards. The proteins were further purified by size-exclusion chromatography using a Superdex 200 Increase 10/300 GL column (GE Healthcare). The selected fractions were pooled and concentrated again for further use.

BioLayer Interferometry binding

The determination of monoclonal antibody binding with S proteins or selected peptides was conducted in an Octet K2 system (ForteBio). The anti-human IgG Fc capture (AHC) biosensors (ForteBio) were used to capture IgG first for 60s. After providing baseline in Octet buffer for another 60s, the sensors were transferred into HCoV S proteins at various concentrations for 120s for association, and into Octet buffer for disassociation for 240s. Alternatively, the hydrated streptavidin biosensors (ForteBio) first captured the N-terminal biotinylated peptides diluted in Octet buffer (PBS plus 0.1% Tween) for 60s, then transferred into Octet buffer for 60s to remove unbound peptide and provide the baseline. Then the sensors were immersed in diluted monoclonal

antibody IgG or Fab for 120s to provide association signal, followed by transferring into Octet buffer to test for disassociation signal for 240s. The data generated was analyzed using the ForteBio Data Analysis software for correction, curve fitting, and calculating the KD values.

Peptide scanning by ELISA binding

N-terminal biotinylated overlapping peptides corresponding to the complete sequence of HCoV-HKU1 S2 subunit (residue number range: 761-1355) were synthesized at A&A Labs (Synthetic Biomolecules). Each peptide was 15 residue long with a 10 amino acid overlap. For ELISA binding, 96-well half-area plates (Corning cat. #3690, Thermo Fisher Scientific) were coated overnight at 4°C with 2 ug/ml of streptavidin in PBS. Plates were washed 3 times with PBS plus 0.05% Tween20 (PBST) and blocked with 3% (wt/vol) bovine serum albumin (BSA) in PBS for 1 hr. After removal of the blocking buffer, the plates were incubated with peptides in 1% BSA plus PBST for 1.5 hr at room temperature. After a washing step, monoclonal antibody or serum samples diluted in 1% BSA/PBST were added into each well and incubated for 1.5 hr. DEN3 human antibody was used as a negative control. After the washes, a secondary antibody conjugated with alkaline phosphatase (AffiniPure goat anti-human IgG Fc fragment specific, Jackson ImmunoResearch Laboratories cat. #109-055-008) diluted 1:1000 in 1% BSA/PBST, was added to each well and incubated for 1 hr. The plates were then washed and developed using alkaline phosphatase substrate pNPP tablets (Sigma cat. #S0942-200TAB) dissolved in stain buffer. The absorbance was recorded at an optical density of 405 nm (OD405) using a VersaMax microplate reader (Molecular Devices), where data were collected using SoftMax software version 5.4.

Cell-cell fusion inhibition assay

HeLa stable cell lines were generated through transduction of lentivirus carrying human ACE2 (hACE2), EGFP, NLS-mCherry, SARS-CoV-1 spike, or SARS-CoV-2 spike. The pBOB construct carrying these genes was co-transfected into HEK293T cells along with lentiviral packaging plasmids pMDL, pREV, and pVSV-G (Addgene #12251, #12253, #8454) by Lipofectamine 2000 (Thermo Fisher Scientific, 11668019) according to the manufacturer's instructions. Supernatants were collected 48h after transfection, then were transduced to pre-seeded HeLa cells. 12h after transduction, stable cell lines were collected, scaled up and stored for cell-cell fusion assay. 10,000 of NLS-mCherry+SARS-COV-1 Spike+ and NLS-mCherry+SARS-COV-2 Spike + cells were seeded into 96-well half-well plate on the day before assay. The culture medium was removed by aspiration before the assay. 50ul of 50ug/ml CC40.8 and DEN3 mAbs were then added to the pre-seeded cells and incubated for 1 hour in an incubator. 50ul of 10,000 EGFP+hACE2+ were added to the plates and incubated for 2 hours before taking images under the microscope.

Sequence alignments and consensus sequence logo generation

The spike sequences of SARS-CoV-2, SARS-CoV-1, RaTG13, RsSHC0144, Rs4081, Pang17, RmYN02, Rf1, WIV1, Yun11, BM48-31, BtKY72, HCoV-HKU1, HCoV-OC43, MERS-CoV, MHV, HCoV-229E and HCoV-NL63 were downloaded from the GenBank and aligned against the SARS-CoV-2 reference sequence using BioEdit (http://www.mbio.ncsu.edu/bioedit/bioedit.html). The frequencies of different residues at positions 1140-1164 was analyzed and sequence logos were generated using the WebLogo 3.0 tool (http:// weblogo.threeplusone.com/) (*3*).

Expression and purification of CC40.8 Fab

To generate Fab, CC40.8 IgG was digested by Papain (SigmaAldrich #P3125) for 4 hours at 37 °C, then was incubated with Protein-A beads at 4 °C for 2 hours to remove the Fc fragments. CC40.8 Fab was concentrated afterwards and further purified by size-exclusion chromatography using a Superdex 200 Increase 10/300 GL column (GE Healthcare). The selected fractions were pooled and concentrated again for further use.

Crystallization and structural determination

A mixture of 9 mg/ml of CC40.8 Fab and 10 × (molar ratio) SARS-CoV-2 stem peptide screened for crystallization using the 384 conditions of the JCSG Core Suite (Qiagen) on our robotic CrystalMation system (Rigaku) at the Scripps Research. Crystallization trials were set-up by the vapor diffusion method in sitting drops containing 0.1 µl of protein and 0.1 µl of reservoir solution. Optimized crystals were then grown in drops containing 0.1 M sodium acetate buffer at pH 4.26, 0.2 M ammonium sulfate, and 28% (w/v) polyethylene glycol monomethyl ether 2000 at 20°C. Crystals appeared on day 7, were harvested on day 15 by soaking in reservoir solution supplemented with 20% (v/v) glycerol, and then flash cooled and stored in liquid nitrogen until data collection. Diffraction data were collected at cryogenic temperature (100 K) at Stanford Synchrotron Radiation Lightsource (SSRL) on the new Scripps/Stanford beamline 12-1, with a beam wavelength of 0.97946 Å, and processed with HKL2000 (*4*). Structures were solved by molecular replacement using PHASER (*5*). A model of CC40.8 was generated by Repertoire Builder (https://sysimm.ifrec.osaka-u.ac.jp/rep_builder/) (*6*). Iterative model building and refinement were carried out in COOT (*7*) and PHENIX (*8*), respectively. Epitope and paratope residues, as well as their interactions, were identified by accessing PISA at the European Bioinformatics Institute (http://www.ebi.ac.uk/pdbe/prot_int/pistart.html) (*9*).

Animal Study

8-Week old Syrian hamsters were given an intraperitoneal (i.p.) antibody injection 12 hours pre-infection. Hamsters were infected through intranasal installation of 10^6 total PFU per animal of SARS-CoV-2 (USA-WA1/2020) in 150uL of DMEM. Hamsters were then weighed for the duration of the study. At day-5 post-infection, animals were sacrificed and lungs were harvested for qPCR viral titer analysis and plaque live virus analysis. The research protocol was approved and performed in accordance with Scripps Research IACUC Protocol #20-0003.

Viral load measurements

SARS-CoV-2 titers were measured by homogenizing organs in DMEM 2% FCS using 100 µm cell strainers (Myriad 2825-8367). Homogenized organs were titrated 1:10 over 6 steps and layered over Vero-E6 cells. After 1 h of incubation at 37°C, a 1% methylcellulose in DMEM overlay was added, and the cells were incubated for 3 days at 37°C. Cells were fixed with 4% PFA and plaques were counted by crystal violet staining.

Statistical Analysis

Statistical analysis was performed using Graph Pad Prism 8 for Mac, Graph Pad Software, San Diego, California, USA. Group of data were compared using the non-parametric unpaired Mann-Whitney-U test. Data were considered statistically significant at $p < 0.05$.

REFERENCES

1. M. Sarzotti-Kelsoe *et al.*, Optimization and validation of the TZM-bl assay for standardized assessments of neutralizing antibodies against HIV-1. *Journal of immunological methods* **409**, 131-146 (2014).
2. L. M. Walker *et al.*, Broad and potent neutralizing antibodies from an African donor reveal a new HIV-1 vaccine target. *Science* **326**, 285-289 (2009).
3. G. E. Crooks, G. Hon, J. M. Chandonia, S. E. Brenner, WebLogo: a sequence logo generator. *Genome Res* **14**, 1188-1190 (2004).
4. Z. Otwinowski, W. Minor, Processing of X-ray diffraction data collected in oscillation mode. *Methods Enzymol* **276**, 307-326 (1997).
5. Afinogenov, Il, [History of the pharmacy of the Main Hospital]. *Voen Med Zh* **318**, 57-60 (1997).
6. D. Schritt *et al.*, Repertoire Builder: high-throughput structural modeling of B and T cell receptors. *Molecular Systems Design & Engineering* **4**, 761-768 (2019).
7. P. Emsley, B. Lohkamp, W. G. Scott, K. Cowtan, Features and development of Coot. *Acta Crystallogr D Biol Crystallogr* **66**, 486-501 (2010).
8. P. D. Adams *et al.*, PHENIX: a comprehensive Python-based system for macromolecular structure solution. *Acta Crystallogr D Biol Crystallogr* **66**, 213-221 (2010).
9. E. Krissinel, K. Henrick, Inference of macromolecular assemblies from crystalline state. *Journal of molecular biology* **372**, 774-797 (2007).
10. J. Ye, N. Ma, T. L. Madden, J. M. Ostell, IgBLAST: an immunoglobulin variable domain sequence analysis tool. *Nucleic acids research* **41**, W34-40 (2013).
11. Y. Cai *et al.*, Distinct conformational states of SARS-CoV-2 spike protein. *Science* **369**, 1586-1592 (2020).
12. M. M. Sauer *et al.*, Structural basis for broad coronavirus neutralization. *bioRxiv*, 2020.2012.2029.424482 (2021).

Table S1. Demographic information of COVID-19 donors

	COVID donor (n = 60)
Age (years)	20–72 (median = 46)
Gender	
Male	47% (28/60)
Female	53% (32/60)
Race/Ethnicity	
White, non-Hispanic	80% (48/60)
Hispanic	8.3% (5/60)
Black, non-Hispanic	1.7% (1/60)
Asian, non-Hispanic	3.3% (2/60)
Unknown	6.7% (4/60)
SARS-CoV-2 PCR Positivity	75% (45/60)
Lateral Flow Positivity	60% (36/60)
Disease Severity	
Mild	56.7% (34/60)
Mild to Moderate	6.7% (4/60)
Moderate	25% (15/60)
Moderate to Severe	5% (3/60)
Severe	5% (3/60)
Critical	1.7% (1/60)
Symptoms	
Cough	60% (36/60)
Fever	55% (33/60)
Fatigue	38.3% (23/60)
Anosmia	31.7% (19/60)
Dyspnea	26.7% (16/60)
Diarrhea	16.7% (10/60)
Days Post Symptom Onset at Collection	6–90 (median = 35.5)

Table S2. X-ray data collection and refinement statistics

Data collection	CC40.8 Fab + SARS-CoV-2 S2 peptide
Beamline	SSRL12-1
Wavelength (Å)	0.97946 Å
Space group	P 2 2_1 2_1
Unit cell parameters	
a, b, c (Å)	54.9, 63.7, 122.0
α, β, γ (°)	90, 90, 90
Resolution (Å) [a]	50.0-1.62 (1.65-1.62)
Unique reflections [a]	54,176 (4,897)
Redundancy [a]	4.3 (3.0)
Completeness (%) [a]	97.0 (89.6)
$\langle I/\sigma_I \rangle$ [a]	29.9 (1.0)
R_{sym} [b] (%) [a]	7.9 (>100)
R_{pim} [b] (%) [a]	2.8 (47.7)
$CC_{1/2}$ [c] (%) [a]	99.4 (56.3)
Refinement statistics	
Resolution (Å)	29.1-1.62
Reflections (work)	54,129
Reflections (test)	1,997
R_{cryst} [d] / R_{free} [e] (%)	17.4/20.6
No. of atoms	3,836
Fab	3,159
Peptide	193
Ligands	35
Solvent	459
Average *B*-values (Å^2)	28
Fab	26
Peptide	34
Ligands	56
Solvent	39
Wilson *B*-value (Å^2)	23
RMSD from ideal geometry	
Bond length (Å)	0.006
Bond angle (°)	1.22
Ramachandran statistics (%)	
Favored	98.2
Outliers	0.0
PDB code	pending

[a] Numbers in parentheses refer to the highest resolution shell.
[b] $R_{sym} = \Sigma_{hkl} \Sigma_i | I_{hkl,i} - \langle I_{hkl} \rangle | / \Sigma_{hkl} \Sigma_i I_{hkl,i}$ and $R_{pim} = \Sigma_{hkl} (1/(n-1))^{1/2} \Sigma_i | I_{hkl,i} - \langle I_{hkl} \rangle | / \Sigma_{hkl} \Sigma_i I_{hkl,i}$, where $I_{hkl,i}$ is the scaled intensity of the i^{th} measurement of reflection h, k, l, $\langle I_{hkl} \rangle$ is the average intensity for that reflection, and *n* is the redundancy.
[c] $CC_{1/2}$ = Pearson correlation coefficient between two random half datasets.
[d] $R_{cryst} = \Sigma_{hkl} | F_o - F_c | / \Sigma_{hkl} | F_o |$ x 100, where F_o and F_c are the observed and calculated structure factors, respectively.
[e] R_{free} was calculated as for R_{cryst}, but on a test set comprising 5% of the data excluded from refinement.

Supplementary Figures and Legends

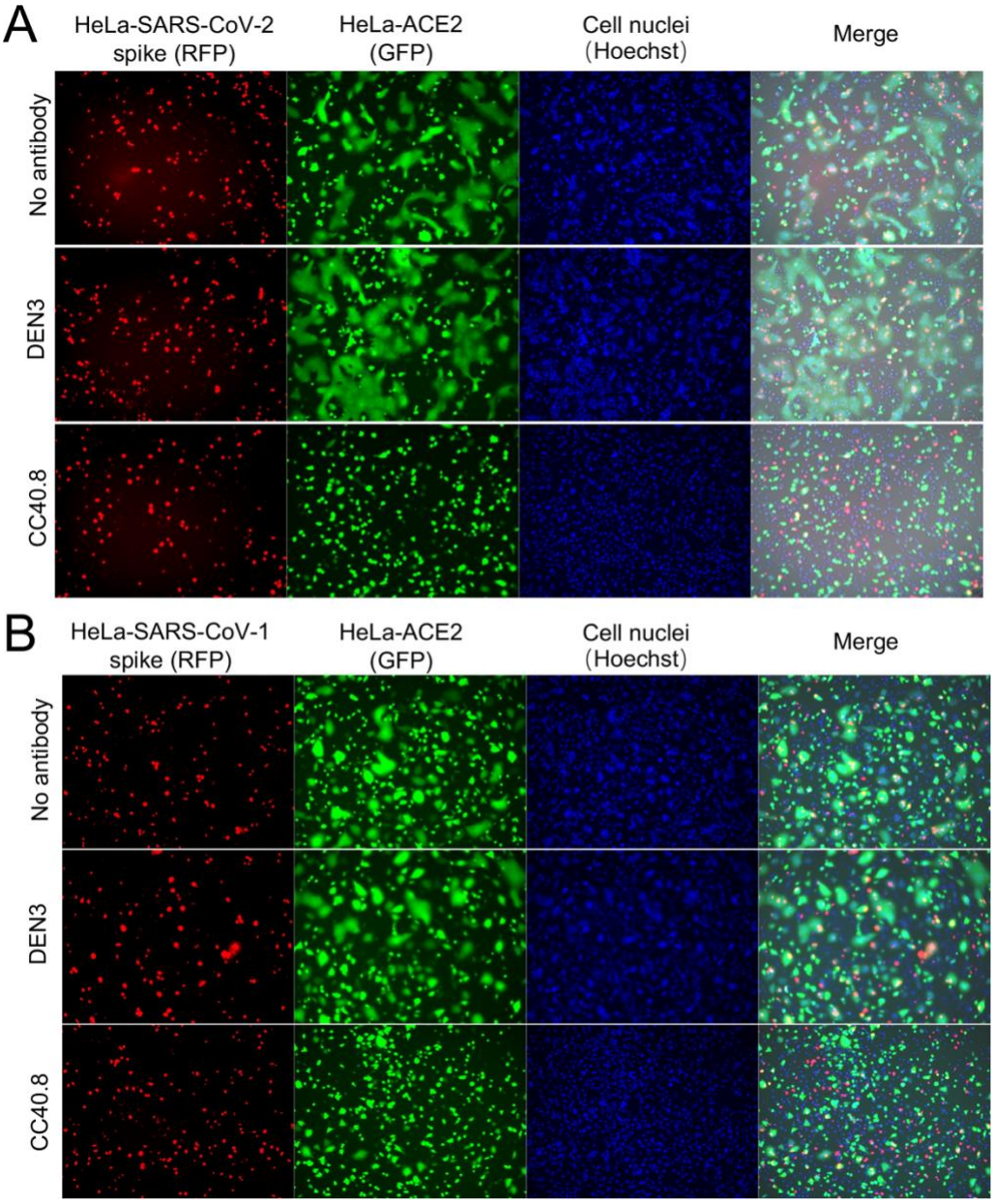

Fig. S1. SARS-CoV-2 & 1 Spike and hACE2 mediated cell-cell fusion inhibition by CC40.8 antibody. HeLa-SARS-CoV-2 & 1 Spike cells expressing nucleus-restricted RFP (red) are pre-incubated with no antibody, negative control antibody (DEN3) or CC40.8 for 1h, and mixed with HeLa-ACE2 cells expressing cytosolic GFP (green). Green syncytia were observed without antibody or with negative control (row 1, 2, 4 & 5), indicating widespread cell-cell fusion mediated by SARS-CoV-1 & 2 spike and hACE2; this was rescued by addition of CC40.8 (row 3 & 6). Hoechst was used to stain cell nuclei.

Peptide number	HKU1 S2 residues	Sequence	OD405nm	
			CC40.8	DEN3
1	761-775	SISASYRFVTFEPFN	0.2	0.2
2	766-780	YRFVTFEPFNVSFVN	0.2	0.2
3	771-785	FEPFNVSFVNDSIES	0.1	0.2
4	776-790	VSFVNDSIESVGGLY	0.1	0.2
5	781-795	DSIESVGGLYEIKIP	0.2	0.2
6	786-800	VGGLYEIKIPTNFTI	0.1	0.2
7	791-805	EIKIPTNFTIVGQEE	0.1	0.2
8	796-810	TNFTIVGQEEFIQTN	0.1	0.2
9	801-815	VGQEEFIQTNSPKVT	0.1	0.2
10	806-820	FIQTNSPKVTIDCSL	0.2	0.2
11	811-825	SPKVTIDCSLFVCSN	0.2	0.2
12	816-830	IDCSLFVCSNYAACH	0.2	0.2
13	821-835	FVCSNYAACHDLLSE	0.2	0.3
14	826-840	YAACHDLLSEYGTFC	0.2	0.3
15	831-845	DLLSEYGTFCDNINS	0.2	0.3
16	836-850	YGTFCDNINSILDEV	0.2	0.2
17	841-855	DNINSILDEVNGLLD	0.1	0.2
18	846-860	ILDEVNGLLDTTQLH	0.1	0.2
19	851-865	NGLLDTTQLHVADTL	0.1	0.2
20	856-870	TTQLHVADTLMQGVT	0.1	0.2
21	861-875	VADTLMQGVTLSSNL	0.1	0.2
22	866-880	MQGVTLSSNLNTNLH	0.1	0.2
23	871-885	LSSNLNTNLHFDVDN	0.1	0.2
24	876-890	NTNLHFDVDNINFKS	0.1	0.2
25	881-895	FDVDNINFKSLVGCL	0.2	0.3
26	886-900	INFKSLVGCLGPHCG	0.2	0.3
27	891-905	LVGCLGPHCGSSSRS	0.2	0.2
28	896-910	GPHCGSSSRSFFEDL	0.2	0.2
29	901-915	SSSRSFFEDLLFDKV	0.2	0.2
30	906-920	FFEDLLFDKVKLSDV	0.1	0.2
31	911-925	LFDKVKLSDVGFVEA	0.2	0.2
32	916-930	KLSDVGFVEAYNNCT	0.2	0.3
33	921-935	GFVEAYNNCTGGSEI	0.2	0.2
34	926-940	YNNCTGGSEIRDLLC	0.2	0.2
35	931-945	GGSEIRDLLCVQSFN	0.2	0.2
36	936-950	RDLLCVQSFNGIKVL	0.2	0.2
37	941-955	VQSFNGIKVLPPILS	0.2	0.2
38	946-960	GIKVLPPILSESQIS	0.2	0.2
39	951-965	PPILSESQISGYTTA	0.2	0.2
40	956-970	ESQISGYTTAATVAA	0.1	0.2
41	961-975	GYTTAATVAAMFPPW	0.2	0.2
42	966-980	ATVAAMFPPWSAAAG	0.1	0.2
43	971-985	MFPPWSAAAGIPFSL	0.2	0.2
44	976-990	SAAAGIPFSLNVQYR	0.2	0.2
45	981-995	IPFSLNVQYRINGLG	0.2	0.2
46	986-1000	NVQYRINGLGVTMDV	0.2	0.2
47	991-1005	INGLGVTMDVLNKNQ	0.1	0.2
48	996-1010	VTMDVLNKNQKLIAT	0.2	0.2
49	1001-1015	LNKNQKLIATAFNNA	0.2	0.2
50	1006-1020	KLIATAFNNALLSIQ	0.2	0.2
51	1011-1025	AFNNALLSIQNGFSA	0.2	0.2
52	1016-1030	LLSIQNGFSATNSAL	0.1	0.2
53	1021-1035	NGFSATNSALAKIQS	0.2	0.2
54	1026-1040	TNSALAKIQSVVNSN	0.2	0.2
55	1031-1045	AKIQSVVNSNAQALN	0.2	0.2
56	1036-1050	VVNSNAQALNSLLQQ	0.2	0.2
57	1041-1055	AQALNSLLQQLFNKF	0.2	0.3
58	1046-1060	SLLQQLFNKFGAISS	0.2	0.2
59	1051-1065	LFNKFGAISSSLQEI	0.2	0.2
60	1056-1070	GAISSSLQEILSRLD	0.2	0.2
61	1061-1075	SLQEILSRLDALEAQ	0.2	0.3
62	1066-1080	LSRLDALEAQVQIDR	0.2	0.2
63	1071-1085	ALEAQVQIDRLINGR	0.2	0.2
64	1076-1090	VQIDRLINGRLTALN	0.2	0.2
65	1081-1095	LINGRLTALNAYVSQ	0.2	0.2
66	1086-1100	LTALNAYVSQQLSDI	0.2	0.3
67	1091-1105	AYVSQQLSDISLVKF	0.2	0.3
68	1096-1110	QLSDISLVKFGAALA	0.2	0.2
69	1101-1115	SLVKFGAALAMEKVN	0.2	0.2
70	1106-1120	GAALAMEKVNECVKS	0.2	0.2
71	1111-1125	MEKVNECVKSQSPRI	0.2	0.3
72	1116-1130	ECVKSQSPRINFCGN	0.2	0.2
73	1121-1135	QSPRINFCGNGNHIL	0.2	0.2
74	1126-1140	NFCGNGNHILSLVQN	0.2	0.2
75	1131-1145	GNHILSLVQNAPYGL	0.2	0.2
76	1136-1150	SLVQNAPYGLLFMHF	0.2	0.3
77	1141-1155	APYGLLFMHFSYKPI	0.2	0.3
78	1146-1160	LFMHFSYKPISFKTV	0.2	0.2
79	1151-1165	SYKPISFKTVLVSPG	0.2	0.2
80	1156-1170	SFKTVLVSPGLCISG	0.2	0.3
81	1161-1175	LVSPGLCISGDVGIA	0.2	0.2
82	1166-1180	LCISGDVGIAPKQGY	0.2	0.2
83	1171-1185	DVGIAPKQGYFIKHN	0.2	0.2
84	1176-1190	PKQGYFIKHNDHWMF	0.2	0.2
85	1181-1195	FIKHNDHWMFTGSSY	0.2	0.3
86	1186-1200	DHWMFTGSSYYYPEP	0.2	0.2
87	1191-1205	TGSSYYYPEPISDKN	0.2	0.2
88	1196-1210	YYPEPISDKNVVFMN	0.2	0.2
89	1201-1215	ISDKNVVFMNTCSVN	0.2	0.2
90	1206-1220	VVFMNTCSVNFTKAP	0.2	0.2
91	1211-1225	TCSVNFTKAPLVYLN	0.2	0.3
92	1216-1230	FTKAPLVYLNHSVPK	0.2	0.2
93	1221-1235	LVYLNHSVPKLSDFE	0.2	0.2
94	1226-1240	HSVPKLSDFESELSH	0.2	0.2
95	1231-1245	LSDFESELSHWFKNQ	2.5	0.2
96	1236-1250	SELSHWFKNQTSIAP	0.2	0.2
97	1241-1255	WFKNQTSIAPNLTLN	0.2	0.2
98	1246-1260	TSIAPNLTLNLHTIN	0.2	0.2
99	1251-1265	NLTLNLHTINATFLD	0.2	0.2
100	1256-1270	LHTINATFLDLYYEM	0.2	0.2
101	1261-1275	ATFLDLYYEMNLIQE	0.2	0.2
102	1266-1280	LYYEMNLIQESIKSL	0.2	0.2
103	1271-1285	NLIQESIKSLNNSYI	0.2	0.2
104	1276-1290	SIKSLNNSYINLKDI	0.2	0.2
105	1281-1295	NNSYINLKDIGTYEM	0.2	0.2
106	1286-1300	NLKDIGTYEMYVKWP	0.2	0.2
107	1291-1305	GTYEMYVKWPWYVWL	0.3	0.3
108	1296-1310	YVKWPWYVWLLISFS	0.3	0.2
109	1301-1315	WYVWLLISFSFIIFL	0.2	0.2
110	1306-1320	LISFSFIIFLVLLFF	0.1	0.2
111	1311-1325	FIIFLVLLFFICCCT	0.2	0.2
112	1316-1330	VLLFFICCCTGCGSA	0.2	0.3
113	1321-1335	ICCCTGCGSACFSKC	0.2	0.3
114	1326-1340	GCGSACFSKCHNCCD	0.2	0.3
115	1331-1345	CFSKCHNCCDEYGGH	0.2	0.2
116	1336-1350	HNCCDEYGGHHDFVI	0.2	0.3
117	1341-1355	EYGGHHDFVIKTSHD	0.2	0.2

Fig. S2. Epitope mapping of CC40.8 antibody with HCoV-HKU1 S2 subunit derived overlapping peptides.

ELISA binding of CC40.8 mAb with HCoV-HKU1 S2 subunit overlapping peptides (residue number range: 761-1355). Each HCoV-HKU1 S2 subunit peptide is 15-residue long with a 10-residue overlap. Peptide IDs, S2 subunit residue number ranges of 15-mer peptides and antibody binding responses are shown. CC40.8 exhibited binding to the 95th peptide (residue position range: 1231-1245) corresponding to the HCoV-HKU1 S2 stem-helix region. DEN3, an unrelated antibody to dengue virus was a control.

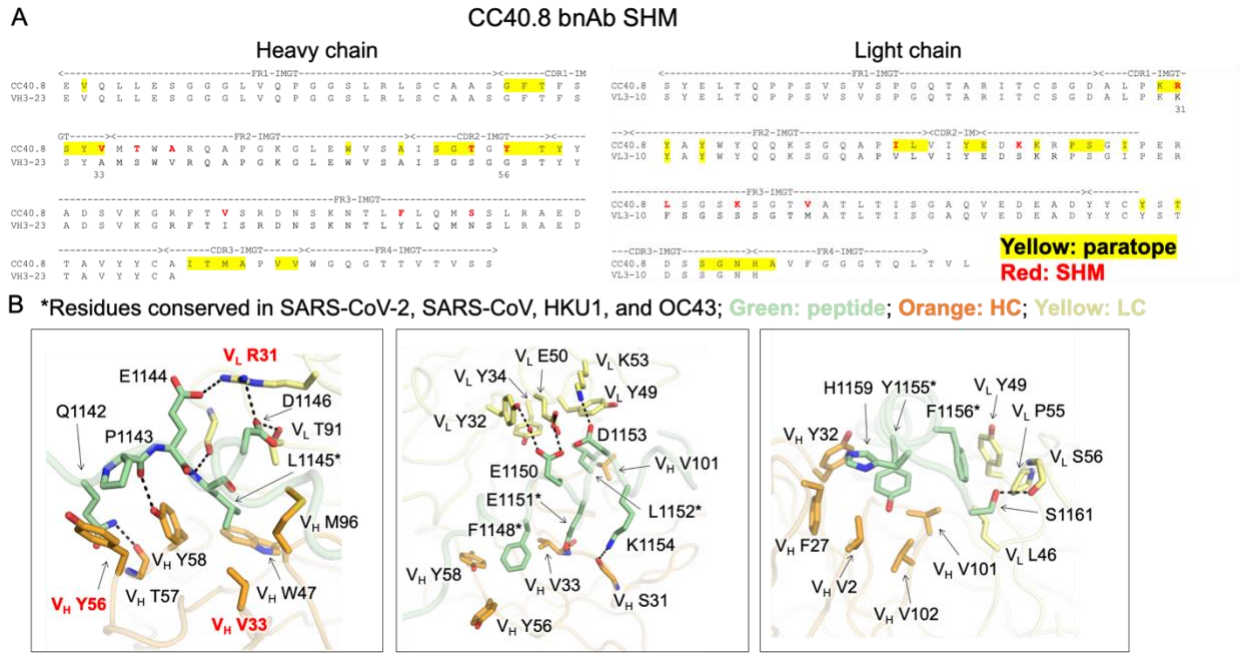

Fig. S3. Contribution of CC40.8 bnAb heavy and light chain germline and somatic mutated V-gene residues in S2 stem epitope recognition.

A. Alignment of CC40.8 with the germline VH3-23 and VL3-10 sequences. Paratope residues [defined as BSA > 0 Å^2 as calculated by PISA (*9*) are highlighted with yellow boxes. Somatically mutated residues as calculated by IgBLAST (*10*) are highlighted in red.

B. Detailed interactions between CC40.8 Fab and the SARS-CoV-2 stem peptide. Heavy and light chains of CC40.8 are shown in orange and yellow, while the SARS-CoV-2 stem peptide is in pale green. Hydrogen bonds and salt bridges are represented by black dashed lines. Somatically mutated residues are shown in red. Conserved residues among coronaviruses are indicated by asterisks (*).

Alanine scanning of SARS-CoV-2 Spike

	SARS-CoV-2	WT	P1140A	L1141A	Q1142A	P1143A	E1144A	L1145A	D1146A	S1147A	F1148A	K1149A	E1150A	E1151
Neutralization	IC50 (ug/ml, CC40.8)	11.5	1.4	0.6	3.3	238.4	14.6	N/A	84.0	20.5	>300	0.6	24.2	>300
	n-fold	1.0	0.1	0.1	0.3	20.7	1.3	N/A	7.3	1.8	>26.11	0.0	2.1	>26.11
BLI Binding	Response Value (CC40.8)	0.61	0.57	N/A	0.59	0.21	0.62	0.02	0.52	0.55	0.35	0.61	0.51	0.07
	% change with WT	100%	95%	N/A	97%	35%	102%	4%	86%	90%	58%	101%	83%	12%
	Response Value (S309)	0.43	0.43	N/A	0.41	0.45	0.42	0.40	0.43	0.45	0.44	0.42	0.48	0.47
	% change with WT	100%	100%	N/A	94%	103%	97%	91%	100%	103%	101%	98%	110%	108%
	SARS-CoV-2	L1152A	D1153A	K1154A	Y1155A	F1156A	K1157A	N1158A	H1159A	T1160A	S1161A	P1162A	D1163A	V1164A
Neutralization	IC50 (ug/ml, CC40.8)	143.1	71.0	4.4	>300	>300	4.7	4.5	6.7	1.9	6.4	11.6	16.0	6.6
	n-fold	12.5	6.2	0.4	>26.11	>26.11	0.4	0.4	0.6	0.2	0.6	1.0	1.4	0.6
BLI Binding	Response Value (CC40.8)	0.65	0.62	0.74	0.34	0.64	0.74	0.65	0.69	0.65	0.49	0.52	0.60	0.75
	% change with WT	108%	102%	122%	55%	106%	122%	107%	114%	107%	81%	86%	99%	124%
	Response Value (S309)	0.48	0.44	0.42	0.46	0.49	0.50	0.43	0.51	0.55	0.47	0.40	0.45	0.47
	% change with WT	110%	101%	98%	107%	113%	114%	99%	117%	127%	108%	93%	103%	110%

Neutralization
n-fold <0.3
n-fold >5

BLI Binding
% change <80%

Alanine scanning of SARS-CoV-1/2 S2 stem peptide

	SARS-CoV-1/2	WT	P1140A	L1141A	Q1142A	P1143A	E1144A	L1145A	D1146A	S1147A	F1148A	K1149A	E1150A	E1151
BLI Binding	Response Value (CC40.8)	3.8	3.5	3.8	3.8	3.7	3.5	0.9	3.3	3.3	2.3	3.7	3.5	0.6
	% change with WT	100%	92%	99%	99%	97%	92%	22%	86%	87%	61%	96%	91%	16%
	SARS-CoV-1/2	L1152A	D1153A	K1154A	Y1155A	F1156A	K1157A	N1158A	H1159A	T1160A	S1161A	P1162A	D1163A	V1164A
BLI Binding	Response Value (CC40.8)	2.9	3.0	3.4	2.1	2.4	3.7	3.0	2.6	3.2	3.3	3.2	2.8	2.5
	% change with WT	76%	80%	89%	54%	62%	97%	79%	68%	84%	87%	83%	74%	66%

Alanine scanning of HCoV-HKU1 S2 stem peptide

	HCoV-HKU1	WT	H1140A	S1141A	V1142A	P1143A	K1144A	L1145A	S1146A	D1147A	F1148A	E1149A	S1150A	E1151A
BLI Binding	Response Value (CC40.8)	4.2	4.6	4.3	4.4	4.4	4.4	3.3	4.4	4.0	4.0	3.6	4.0	1.7
	% change with WT	100%	110%	104%	105%	106%	105%	79%	105%	96%	96%	87%	96%	41%
	HCoV-HKU1	L1152A	S1153A	H1154A	W1155A	K1156A	F1157A	N1158A	Q1159A	T1160A	S1161A	I1162A	A1163A	P1164A
BLI Binding	Response Value (CC40.8)	3.7	4.0	3.8	1.8	2.7	4.5	4.2	4.2	4.3	4.3	4.3	4.2	3.8
	% change with WT	88%	96%	91%	43%	64%	107%	101%	100%	104%	104%	104%	100%	91%

Fig. S4. Epitope mapping of CC40.8 bnAb by alanine scanning mutagenesis of SARS-CoV-2 spike and SARS-CoV-2/HCoV-HKU1 S2 stem peptides using neutralization and BLI binding assays.

The upper panel shows the IC50 neutralization of CC40.8 bnAb with WT SARS-CoV-2 and spike mutant pseudoviruses and the BLI binding responses with WT SARS-CoV-2 soluble S protein and alanine mutants. SARS-CoV-2 receptor binding domain (RBD) antibody S309 was control for the spike binding assays. The IC50 fold change (n-fold) was calculated by dividing the mutant value by the WT value. For IC50, n-fold <0.3 are indicated in red, n-fold >5 in green. The middle and lower panels show BLI binding responses of CC40.8 antibody to WT and alanine mutants of the SARS-CoV-1/2 and HCoV-HKU1 stem peptides, respectively. For binding response values where the % change in binding (from WT peptide) is <80%, are indicated in yellow. Antibody S309 recognizing the RBD of both SARS-CoV-1 and SARS-CoV-2 was used as control. N/A, not available.

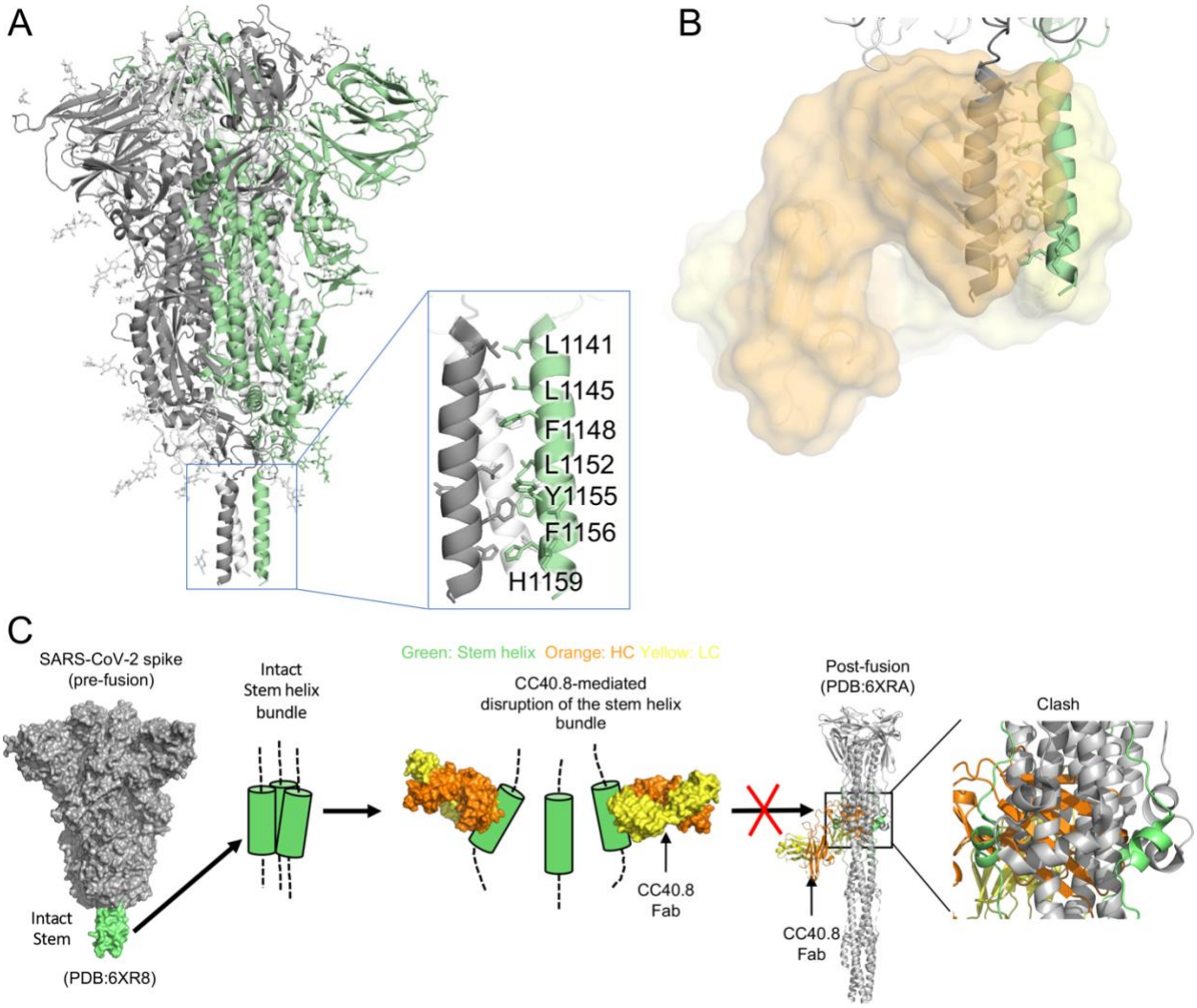

Fig. S5. CC40.8 binds to a buried interface of the 3-helix bundle and the predicted mechanism of neutralization.

A. A SARS-CoV-2 spike structure in pre-fusion state. The three protomers are shown in gray, pale green, and white, respectively with N-linked glycans represented by sticks. The 3-helix bundle stem region is highlighted in a blue-outlined box. Representative epitope residues of CC40.8 are shown in sticks. CC40.8 bnAb epitope is rich in hydrophobic residue. A cryo-EM structure of SARS-CoV-2 spike structure in pre-fusion state that contains the coordinates of the 3-helix bundle stem region (PDB: 6XR8, (*11*)) is shown here.

B. SARS-CoV-2 spike pre-fusion structure superimposed with the structure of CC40.8 (orange/yellow) in complex with a SARS-CoV-2 S2 peptide. CC40.8 would clash with the other protomers of the spike protein in pre-fusion state.

C. A putative neutralization mechanism of CC40.8. The S2 3-helix bundle region is shown in green, whereas heavy and light chains of CC40.8 in orange and yellow, respectively. Mechanism of neutralization model inspired by interaction of a mouse S2 stem antibody, B6, isolated from an S protein vaccinated animal that targets a similar stem epitope (*12*).